




Photon vortex generation by synchrotron radiation experiments in relativistic quantum approach

Tomoyuki Maruyama ^{1,2,*} Takehito Hayakawa ^{3,4,†} Ryoichi Hajima ³ Toshitaka Kajino,^{5,6,7} and Myung-Ki Cheoun⁸¹College of Bioresource Sciences, Nihon University, Fujisawa 252-0880, Japan²Tokyo Metropolitan University, Hachioji, Tokyo 181-8588, Japan³Kansai Institute for Photon Science, National Institutes for Quantum Science and Technology, Kizugawa, Kyoto 619-0215, Japan⁴Institute of Laser Engineering, Osaka University, Suita, Osaka 565-0871, Japan⁵Beihang University, School of Physics, International Research Center for Big-Bang Cosmology and Element Genesis,

Peng Huanwu Collaborative Center for Research and Education, Beijing 100083, China

⁶National Astronomical Observatory of Japan, 2-21-1 Osawa, Mitaka, Tokyo 181-8588, Japan⁷Graduate School of Science, The University of Tokyo, 7-3-1 Hongo, Bunkyo-ku, Tokyo 113-033, Japan⁸Department of Physics and OMEG Institute, Soongsil University, Seoul 156-743, Korea

(Received 30 June 2023; accepted 7 November 2023; published 26 December 2023)

We formulate a theoretical approach to describe photon vortex production in synchrotron/cyclotron radiation from a helical moving electron under a uniform magnetic field in the relativistic quantum framework. In quantum theory, electron orbitals in a magnetic field are under Landau states. The Landau level density increases with decreasing the magnetic field strength, and it is practically impossible to calculate exactly the synchrotron radiation in possible magnetic fields in the laboratory. We present a method to calculate it by using asymptotic formulations of the emission amplitudes under the condition of $L_i - L_f \ll L_i$, where L_i and L_f are the initial and final Landau numbers, respectively. The wave function of the generated photon is the eigenstate of the z component of the total angular momentum (zTAM) when the magnetic field is parallel to the z axis. The approximation is applicable for photon vortex production of several tens \hbar of zTAM. We also calculate numerically the energy spectra and spatial distribution of photon vortices in magnetic field strengths of 10 and 20 T using electrons with energies of 150 MeV and 8 GeV and Larmor radii of 10 and 100 μm for the helical motion. Although the Landau number becomes up to 10^8 in these conditions, the radiations could be calculated using the approximation. The results indicate that it is possible to produce predominantly photon vortices with a fixed zTAM when we control the energy and entrance trajectory of electrons and the structure of a magnetic field. The present formula contributes to the prediction and verification of photon vortex generation.

DOI: [10.1103/PhysRevResearch.5.043289](https://doi.org/10.1103/PhysRevResearch.5.043289)

I. INTRODUCTION

Since Allen *et al.* proposed optical vortices [1], this theme has been advancing in fundamental science [2–6] and various applications [7–13] such as the transmission of enormous amounts of information [13] and the formation of chiral structures in solids [12]. The possible origin of optical vortices in a natural phenomenon has also been discussed. For example it was suggested that optical vortices are generated from rotating black holes [14]. At present, optical vortices are mainly generated using laser with various optical devices to provide for various experiments. On the other hand, it was proposed that optical vortices could be generated by harmonic radiations in synchrotron radiations of electrons with a

helical undulator, which produces circular polarized light by the fundamental radiation, and it is expected that n th harmonic radiations are optical vortices having an average angular momentum of $n\hbar$ per photon [15]. Generation of optical vortices using helical undulators has been studied experimentally and theoretically [16–22]. Furthermore, optical vortex generation by free electron lasers with electron beams has been demonstrated [23,24].

Allen *et al.* [1] also pointed out that a single photon can have the wave function of a vortex at the quantum level [1]. The generation of photon vortices was experimentally verified using quantum entanglement [25,26]. One of the remarkable features of the photon vortex is that the wave function of the photon vortex is the eigenstate of the z component of the total angular momentum (zTAM) when the photon propagates along the z direction. This means that a single photon vortex can have many different states for zTAM whereas photons described well by a plane wave can have only two states of helicity $+s$ and $-s$. This feature is useful for quantum communications [7,9]. Furthermore, using photon vortices with a large zTAM, one could observe quantum effect caused by the large angular momentum transfer in interactions between individual photons and quantum objects such as molecules

*maruyama.tomoyuki@nihon-u.ac.jp

†hayakawa.takehito@qst.go.jp

Published by the American Physical Society under the terms of the [Creative Commons Attribution 4.0 International](https://creativecommons.org/licenses/by/4.0/) license. Further distribution of this work must maintain attribution to the author(s) and the published article's title, journal citation, and DOI.

[27,28], atoms [29,30], and atomic nuclei [31]. It has been discussed that when a high- z TAM photon vortex interacts on a nucleus its nuclear reaction is different from that with a plane-wave photon [31,32]. For the photon vortex, the wave functions based on Laguerre-Gaussian [6] and Bessel functions [33] have been theoretically predicted and these wave functions have the features as explained above.

Even if an optical vortex is generated at the macrolevel, it does not necessarily mean that the wave function of each photon consisting of the initial nonvortex light is converted to the wave function of the eigenstate of z TAM. Generation of photon vortices requires a mechanism in which the wave function of the initial nonvortex photon is converted to the vortex wave function or newly produces a photon with a vortex wave function. Among known generation mechanisms for the optical vortex, harmonic radiations from a spiral moving electron under a magnetic field [15–21] and nonlinear Compton scattering on an electron with a circularly polarized high-flux laser [32,34,35] are two of the candidates for a mechanism for efficient generation of photon vortices and controlling of the quantum states of the generated photon vortices, because they are fundamental processes; in the former a single electron under a magnetic field radiates a photon, whereas in the latter an electron absorbs multiphotons and radiates a photon. It is possible to treat these processes in the framework of quantum theory and to predict the properties of generated photon vortices such as energy and z TAM.

Recently, we have presented the photon vortex generation by synchrotron/cyclotron radiations from spiral moving electrons in an extremely strong uniform magnetic field with a strength of 10^8 – 10^{10} T, which could be realized in celestial systems such as neutron stars [36] and black holes [37], using calculation taking Landau quantization into account [38]. In the quantum framework, the electron orbitals under magnetic fields are in Landau quantization [39–45], and a photon is radiated through a transition of an electron between two different Landau levels. In uniform magnetic fields, electrons make helical motions and their wave functions are the eigenstates of the angular momentum component along the direction parallel to the magnetic field. As predicted previously [19], our previous study [38] also shows that n th harmonic radiations from electrons under a uniform magnetic field are photon vortices of the eigenstate with z TAM of $n\hbar$. Furthermore, the calculated energy spectra show that the energy region of each mode photon vortex is limited and photon vortices dominate in the energy region higher than the maximum energy of the fundamental radiation being the nonphoton vortex. This result indicates that it is possible to generate predominantly photon vortices with a specific z TAM when we control the structure of a magnetic field and the entrance trajectory of the initial electrons for the magnet system.

The previous experiments using helical undulators have verified generation of optical vortices [16–18], where the vortex shape appears in the interference between the produced light and fundamental light. In these experiments, however, they did not show clearly behaviors of photon vortices with a fixed angular momentum. Furthermore, there is another problem in the experimental verification. In the quantum theory with Landau quantization, the decay widths of radiated photons depend on the wave functions of the initial and final

electron states [41]. Therefore, the decay probabilities and energy spectra of radiated photons depend on the structure of the magnetic field. The helical undulators have been widely used for generation of circularly polarized light in synchrotron radiation facilities on the ground, but it consists of an array of magnets for a periodically alternating field to produce a spiral motion of electrons and the structure of the magnetic field is different from the uniform magnetic field. Therefore, observation using helical undulators is, in principle, different from that for uniform magnetic fields.

The aim of this paper is to present a method using Landau quantization for calculating photon vortex generation with electron beams under possible conditions on the ground. In the extremely strong magnetic fields of 10^8 – 10^{10} T in the universe, the level density of Landau states is low enough to calculate exactly the synchrotron radiations [38]. However, the level density increases as the magnetic field strength becomes weaker. In experiments on the ground, the possible strength of the magnetic field is as weak as the order of 10 T so that the Landau level number for a Larmor radius of approximately $10\ \mu\text{m}$ becomes larger than 10^5 . It is practically impossible to perform exactly a calculation with such huge Landau level numbers in the framework of Ref. [38]. Thus, we need another approach to calculate numerically the properties of generated photon vortices. In this paper we exhibit an approximate method for this calculation. Even if the Landau quantum number is very large, this approximation is reasonable for generation of the photon vortices with low angular momenta. Therefore, we calculate the photon vortex production in the quantum mechanical framework and show production probabilities, energy spectrum, and spatial distribution of photon vortices.

II. FORMALISM

In this section we briefly explain our formalism, the details of which are written in Ref. [38]. In the present paper, we consider a uniform dipole magnetic field along the z direction, $\mathbf{B} = (0, 0, B)$, by which an electron trajectory draws a circle in a plane perpendicular to the z direction under this magnetic field. We use the natural unit $\hbar = c = 1$. The electron wave function $\psi(\mathbf{r})$ at the position $\mathbf{r} = (x, y, z)$ in this system is obtained from the following Dirac equation:

$$\{\boldsymbol{\alpha} \cdot (-i\nabla_{\mathbf{r}} + e\mathbf{A}) + \beta m_e - E\}\psi(\mathbf{r}) = 0, \quad (1)$$

where $\boldsymbol{\alpha}$ and β are the Dirac matrices, \mathbf{A} is an electromagnetic vector potential, E is the electron energy, e is the elementary charge, and m_e is the electron mass. We choose the symmetry gauge with the vector potential being $\mathbf{A} = (-y, x, 0)B/2$. In order to describe a solution of Eq. (1), we introduce the two-dimensional harmonic wave function with the cylindrical coordinate as

$$\begin{aligned} G_n^L(\mathbf{r}_T) &\equiv R_n^L(r_T) \frac{e^{i\phi}}{\sqrt{2\pi}} \\ &= \sqrt{\frac{2n!}{(n+|L|)!}} r_T^{|L|} e^{-r^2/2} \mathcal{L}_n^{|L|}(r_T^2) \frac{e^{iL\phi}}{\sqrt{2\pi}} \end{aligned} \quad (2)$$

where $\mathcal{L}_n^{|L|}$ is the associated Laguerre function, L is the z component of the orbital angular momentum (z OAM), p_z is

the z component of the momentum, and n is the number of the node.

A solution of Eq. (1) in this system is known as follows [41]:

$$\begin{aligned} \psi(\mathbf{r}) = & \left\{ \frac{1 + \Sigma_z}{2} G_{n'}^{L-1} \left(\sqrt{\frac{eB}{2}} \mathbf{r}_T \right) + \frac{1 - \Sigma_z}{2} G_n^L \left(\sqrt{\frac{eB}{2}} \mathbf{r}_T \right) \right\} \\ & \times \sqrt{\frac{E + m_e}{2E}} \begin{bmatrix} \chi_h \\ \frac{\hat{p} \cdot \boldsymbol{\sigma}}{E + m_e} \chi_h \end{bmatrix} \frac{e^{ip_z z}}{\sqrt{R_z}}, \\ \tilde{\mathbf{p}} = & (0, \sqrt{2eBN_L}, p_z), \end{aligned} \quad (3)$$

where R_z is the size of the system along the z direction, $\boldsymbol{\sigma} \equiv (\sigma_x, \sigma_y, \sigma_z)$ is the Pauli matrix, χ_h is the two-dimensional Pauli spinor satisfying $\sigma_z \chi_h = h \chi_h$ ($h = \pm 1$), $\Sigma_z = \text{diag}(1, -1, 1, -1)$, and $n' = n$ when $L \geq 0$ and $n' = n - 1$ when $L \leq -1$. The wave function is the eigenstate of the zTAM the value of which is $J = L + h/2$. The electron energy in a Landau level is given by $E = \sqrt{2eBN_L + p_z^2 + m_e^2}$ where N_L indicates the Landau quantum number defined as $N_L = (L + |L|)/2 + n$. The form of χ_h is arbitrary when $N_L \geq 1$ because there are two degenerate states at fixed L and n , whereas the state with $N_L = 0$, which is the so called lowest Landau state, is not degenerate and its spinor is taken to be only $\chi_{-1} = (0, 1)$. The wave function for $n = 0$ corresponds to the helical motion along the z axis when $L \geq 0$, whereas the wave function for $n \geq 1$ indicates the helical motion along an axis that is different from the initial axis [46].

Next, we consider one photon emission from an electron through a transition between two Landau states. We restrict only $L \geq 0$ and $n = 0$ states for the initial and final states which correspond to electrons rotating along the z axis. We define the z components of the initial and final momentum as p_{iz} and p_{fz} , respectively. We also define the zOAM of the initial and final states as L_i and L_f , and spin states h_i and h_f , which indicate the zTAM of the initial and final states as $J_i = L_i + s_i$ and $J_f = L_f + h_f$. In these conditions we can consider only photons with zTAM $K = J_i - J_f$ and propagating along the z direction with the z component of momentum $q_z = p_{iz} - p_{fz}$. Thus, a wave function of an emitted photon is obtained as a solution of the Klein-Gordon equation written as

$$-\nabla^2 \mathbf{A}(\mathbf{r}) = -(\nabla_z^2 + \nabla_T^2) \mathbf{A}(\mathbf{r}) = (q_z^2 - \nabla_T^2) \mathbf{A}(\mathbf{r}) = e_q^2 \mathbf{A}(\mathbf{r}), \quad (4)$$

where e_q is the photon energy. Here, we choose the Coulomb gauge $\nabla \cdot \mathbf{A} = 0$ with the photon as $A_0 = 0$. There are two orthogonal states, which are the so called transverse magnetic (TM) state and the transverse electric (TE) state at fixed m [33], the wave functions of which are written as

$$\mathbf{A}_m^{(\text{TM})} = \frac{1}{2e_q} e^{i(q_z z - e_q t)}$$

$$\times [iq_z(\tilde{J}_{m+1} - \tilde{J}_{m-1}), q_z(\tilde{J}_{m+1} + \tilde{J}_{m-1}), 2q_T \tilde{J}_m],$$

$$\mathbf{A}_m^{(\text{TE})} = \frac{1}{2} e^{i(q_z z - e_q t)} [i(\tilde{J}_{m+1} + \tilde{J}_{m-1}), (\tilde{J}_{m+1} - \tilde{J}_{m-1}), 0] \quad (5)$$

with

$$\tilde{J}_M(\mathbf{r}_T) = J_M(q_T r_T) e^{iM\phi}, \quad (6)$$

where $q_T = \sqrt{e_q^2 - q_z^2}$, and J_M is the Bessel function. Furthermore, we have another choice for the orthogonal states as $\mathbf{A}_{m,s} = -i(\mathbf{A}_m^{(\text{TE})} - s\mathbf{A}_m^{(\text{TM})})/\sqrt{2}$ ($s = \pm 1$) [20], which are equivalent to the states of the helicity $s = \pm 1$ at the limit of $q_T \rightarrow 0$ as

$$\mathbf{A}_{m,s}(\mathbf{r}, t) \rightarrow \frac{1}{\sqrt{\Omega_R}} \boldsymbol{\epsilon}_s e^{i(m-s)\phi} e^{i(q_z z - e_q t)}, \quad (7)$$

with $\boldsymbol{\epsilon}_s = (1, is, 0)/\sqrt{2}$ and Ω_R being the system volume.

The decay width of the electron at an initial state i is obtained as

$$\begin{aligned} \Gamma_e(i) = & \frac{e^2}{8\pi^2} \sum_{f,m,\alpha} \int \frac{dq_z dq_T q_T}{e_q} \frac{dp_{fz}}{2\pi} \delta(E_i - E_f - e_q) \\ & \times \left| \int d\mathbf{r} \bar{\psi}_f(\mathbf{r}) \mathcal{A}_m^{(\alpha)*}(\mathbf{r}) \psi_i(\mathbf{r}) \right|^2, \end{aligned} \quad (8)$$

where f indicates the final electron state, and $E_f = \sqrt{2eBN_f + (p_{iz} - q_z)^2 + m_e^2}$. Substituting Eqs. (3) and (5) into Eq. (8), we can obtain the detailed expression of the decay width. To get the detailed expression, we define

$$\begin{aligned} \mathcal{M} \left(L_f, n_f; L_i, n_i; \frac{q_T}{\sqrt{eB}} \right) \\ = \frac{eB}{2} \int d\mathbf{r}_T r_T R_{n_f}^{L_f} (eB r_T^2 / 2) J_{L_f - L_i}(q_T r_T) R_{n_i}^{L_i} (eB r_T^2 / 2) \end{aligned} \quad (9)$$

and write $\mathcal{M}_{22} = \mathcal{M}(L_f, n_f; L_i, n_i)$, $\mathcal{M}_{11} = \mathcal{M}(L_f - 1, n_f; L_i - 1, n_i)$, $\mathcal{M}_{21} = \mathcal{M}(L_f, n_f; L_i - 1, n_i)$, and $\mathcal{M}_{12} = \mathcal{M}(L_f - 1, n_f; L_i, n_i)$. We make the average of the strengths in Eq. (8) for the initial spin and the summation for the final spin. We finally obtain the decay width of

$$\begin{aligned} \frac{d\Gamma_e}{dq_z} = & \frac{1}{2} \sum_{s_i, s_f} \sum_a \frac{d\Gamma_{if}^{(a)}}{dp_{fz}} \\ = & \frac{\alpha_e (E_f + m_e)(E_i + m_e)}{2\pi E_i E_f} \sum_a \text{Tr}[\mathcal{T}_a^\dagger \mathcal{T}_a] \end{aligned} \quad (10)$$

with

$$\begin{aligned} \mathcal{T}_{\text{TM}} = & \frac{q_z}{2e_q} \left\{ \mathcal{M}_{12} \begin{bmatrix} \frac{p_{iT}}{E_i + m_e} & \frac{ip_{iz}}{E_i + m_e} - \frac{ip_{fz}}{E_f + m_e} \\ 0 & \frac{p_{fT}}{E_i + m_e} \end{bmatrix} - \mathcal{M}_{21} \begin{bmatrix} -\frac{p_{iT}}{E_f + m_e} & 0 \\ \frac{ip_{fz}}{E_f + m_e} - \frac{ip_{iz}}{E_i + m_e} & -\frac{p_{iT}}{E_i + m_e} \end{bmatrix} \right\} \\ & + \frac{q_T}{e_q} \left\{ \mathcal{M}_{11} \begin{bmatrix} \frac{p_{iz}}{E_i + m_e} + \frac{p_{fz}}{E_f + m_e} & -\frac{ip_{iT}}{E_i + m_e} \\ \frac{ip_{fT}}{E_f + m_e} & 0 \end{bmatrix} + \mathcal{M}_{22} \begin{bmatrix} 0 & \frac{ip_{fT}}{E_f + m_e} \\ -\frac{ip_{iT}}{E_i + m_e} & \frac{p_{iz}}{E_i + m_e} + \frac{p_{fz}}{E_f + m_e} \end{bmatrix} \right\}, \end{aligned} \quad (11)$$

$$\mathcal{T}_{TE} = \mathcal{M}_{12} \begin{bmatrix} \frac{p_{iT}}{E_i+m_e} & \frac{ip_{iz}}{E_i+m_e} - \frac{ip_{fz}}{E_f+m_e} \\ 0 & \frac{p_{fT}}{E_i+m_e} \end{bmatrix} + \mathcal{M}_{21} \begin{bmatrix} -\frac{p_{fT}}{E_f+m_e} & 0 \\ \frac{ip_{fz}}{E_f+m_e} - \frac{ip_{iz}}{E_i+m_e} & -\frac{p_{iT}}{E_i+m_e} \end{bmatrix}, \tag{12}$$

where $p_{i(f)T} = \sqrt{2eB\bar{N}_{i(f)}}$. Note that the possible energy of an emitted photon with m is limited by

$$\frac{eBm}{E_i + |p_{iz}|} \leq e_q \leq \frac{eBm}{E_i - |p_{iz}|}. \tag{13}$$

In this paper we are interested in the emission of the photon with the zTAM $m = 1-5$, which is much smaller than zTAM of the initial and final electrons. Then, we consider the approximate expression of the decay width of Eq. (10). As mentioned before, the wave function for $n = 0$ and $L \geq 0$ corresponds to the helical motion along the z axis, whereas the wave function for $n \geq 1$ and/or $L \leq -1$ indicates the helical motion along an axis that is different from the initial axis [46]. Then, we take only $n = 0$ for the initial state. As shown in Ref. [38], in addition, contributions from $n_f \geq 1$ are very small in the energy region where the photon vortex with a small zTAM is emitted, so that we can restrict $n_i = n_f = 0$ though we examine contributions from $n_f = 1$ later.

The associated Laguerre functions, $\mathcal{L}_n^p(x)$, when $n = 0$ and 1 are written as

$$\mathcal{L}_0^L(x) = 1, \quad \mathcal{L}_1^L(x) = 1 - L + r^2. \tag{14}$$

When $L_i \geq L_f \geq 0$, then,

$$\begin{aligned} \mathcal{M}\left(L_f, 0; L_i, 0; \frac{q_T}{\sqrt{eB}}\right) &= \frac{eB}{\sqrt{L_i!L_f!}} \int dr r e^{-r^2/2eB} \left(\sqrt{\frac{eB}{2}}r\right)^{L_i+L_f} J_{L_i-L_f}(q_T r) \\ &= \sqrt{\frac{L_f!}{L_i!}} \left(\frac{q_T^2}{2eB}\right)^{(L_i-L_f)/2} e^{-q_T^2/2eB} \mathcal{L}_{L_f}^{L_i-L_f}\left(\frac{q_T^2}{2eB}\right) = \sqrt{\frac{1}{2}} e^{-q_T^2/4eB} R_{L_f}^{L_i-L_f}\left(\sqrt{\frac{q_T^2}{2eB}}\right), \end{aligned} \tag{15}$$

and

$$\begin{aligned} \mathcal{M}(L_f, 1; L_i, 0) &= \frac{eB}{2\sqrt{L_i!(L_f+1)!}} \int dr r e^{-r^2/2eB} \left(\sqrt{\frac{eB}{2}}r\right)^{L_i+L_f} (1+L_f-eBr^2)J_{L_i-L_f}(q_T r) \\ &= \frac{1}{2}\sqrt{\frac{(L_f+1)!}{L_i!}} \left(\frac{q_T^2}{2eB}\right)^{(L_i-L_f)/2} e^{-q_T^2/2eB} \left\{ \mathcal{L}_{L_f}^{L_i-L_f}\left(\frac{q_T^2}{2eB}\right) - \mathcal{L}_{L_f+1}^{L_i-L_f}\left(\frac{q_T^2}{2eB}\right) \right\} \\ &= \frac{1}{2\sqrt{2}} e^{-q_T^2/4eB} \left\{ \sqrt{L_f+1} R_{L_f}^{L_i-L_f}\left(\frac{q_T^2}{\sqrt{2eB}}\right) - R_{L_f+1}^{L_i-L_f}\left(\frac{q_T}{\sqrt{2eB}}\right) \right\}. \end{aligned} \tag{16}$$

As mentioned above, in experiments on the ground the zOAM of initial and final electrons must require the condition that $L_i > L_f \gg L_g \equiv L_i - L_f$, and we can use the following asymptotic formula [47] as

$$\mathcal{L}_n^m(x) \approx e^{x/2} (nx)^{-m/2} J_m(2\sqrt{nx}) \quad (n \gg m), \tag{17}$$

which leads to

$$R_n^m(x) \approx \sqrt{\frac{2n!}{(n+m)!}} n^{m/2} J_m(2\sqrt{nx}) \approx e^{-m/2n} J_m(2\sqrt{nx}), \tag{18}$$

when $n \gg m$ and x is fixed. When $L_g \equiv L_i - L_f \ll L_i$, then, we obtain the following approximate equations of the transition matrix \mathcal{M} up to the lowest order of L_g/L_i as

$$\begin{aligned} \mathcal{M}(L_f, 0; L_i, 0) &\approx \sqrt{\frac{L_i!}{(L_i+L_g)!}} L_i^{-L_g/2} e^{-\frac{q_T^2}{4eB}} J_{L_g} \approx e^{-\frac{L_g^2}{2L_i} - \frac{q_T^2}{4eB}} J_{L_g} \left(\sqrt{\frac{2L_i}{eB}} q_T\right), \\ \mathcal{M}(L_f, 1; L_i, 0) &\approx \frac{1}{2} e^{-q_T^2/4eB} \left\{ \sqrt{L_f+1} e^{-\frac{L_g^2}{2L_f}} J_{L_g} \left(\sqrt{\frac{2L_f}{eB}} q_T\right) - \sqrt{L_i+1} e^{-\frac{L_g^2}{2(L_f+1)}} J_{L_g} \left(\sqrt{\frac{2(L_f+1)}{eB}} q_T\right) \right\} \\ &\approx \frac{1}{2} e^{-\frac{L_g^2}{2L_f} - \frac{q_T^2}{4eB}} \left\{ \left[\sqrt{L_i} - \frac{L_g+1}{\sqrt{2L_i}} \right] J_{L_g} \left(\sqrt{\frac{2L_f}{eB}} q_T\right) - \sqrt{L_i} \left(1 + \frac{L_g^2+1}{2L_i^2}\right) \left[J_{L_g} \left(\sqrt{\frac{2L_f}{eB}} q_T\right) \right] \right\} \end{aligned} \tag{19}$$

$$\begin{aligned}
 & + \frac{L_q}{2L_f} J_{L_g} \left(\sqrt{\frac{2L_f}{eB}} q_T \right) - \frac{q_T}{\sqrt{2L_f eB}} J_{L_g+1} \left(\sqrt{\frac{2L_f}{eB}} q_T \right) \Bigg\} \\
 & \approx \frac{1}{2} e^{-\frac{L_g^2}{2L_i} - \frac{q_T^2}{4eB}} \left[\frac{q_T}{\sqrt{2eB}} J_{L_g+1} \left(\sqrt{\frac{2L_i}{eB}} q_T \right) - \frac{L_g}{\sqrt{L_i}} J_{L_g} \left(\sqrt{\frac{2L_i}{eB}} q_T \right) \right]. \tag{20}
 \end{aligned}$$

To examine the above approximate calculation with the asymptotic expression, we show the results of $\mathcal{M}(L_i, 0; L_f, 0)$ with the approximate formula Eq. (19) and those with the exact formula Eq. (15) when $L_i = 200$ and $L_i - L_f = L_g = 2$ (a), $L_g = 5$ (b), and $L_g = 10$ (c) in Fig. 1. The results in the approximated expression (solid lines) well agree those in the exact one (dotted lines) when $L_g = 2$ and 5, while the two results are slightly different around the peaks when $L_g = 10$. In this paper we treat the condition that $L_i \approx 10^5 - 10^8$, where the above asymptotic form is applicable for production of photon vortices with zTAM of up to several tens. In addition, we confirm that the expression with the asymptotic formula is as valid for $n_f = 1$ as for $n_f = 0$ though we omitted $n_f = 1$ here. Furthermore, we also set the condition that $\sqrt{2eBL_i} \ll E_i$, which causes $E_i \gg e_q$, and obtain the photon energy e_q with

$$e_q = \sqrt{2eBL_i + p_{iz}^2 + m_e^2} - \sqrt{2eB(L_i - L_g) + (p_{iz} - q_z)^2 + m_e^2} \approx \frac{eBL_g + p_{iz}q_z}{E_i},$$

which leads to

$$q_z \approx \frac{E_i e_q - eBL_g}{p_{iz}}. \tag{21}$$

In addition, we use the approximations as $\mathcal{M}_{11} \approx \mathcal{M}_{22}$ and

$$\frac{p_{iz}}{E_i + m_e} - \frac{p_{fz}}{E_f + m_e} \approx \frac{q_z}{E_i + m_e} - \frac{p_{iz}e_q}{(E_i + m_e)^2} \equiv \Delta Z_{if}, \tag{22}$$

$$\frac{\sqrt{2eBL_i}}{E_i + m_e} - \frac{\sqrt{2eBL_f}}{E_f + m_e} \approx \frac{\sqrt{eBL_g}}{\sqrt{2L_i}(E_i + m_e)} - \frac{\sqrt{2eBL_i}e_q}{(E_i + m_e)^2} \equiv \Delta T_{if}. \tag{23}$$

Thus, we substitute the above approximate equations into Eqs. (11) and (12) and obtain the following equations for \mathcal{T}_{TE} and \mathcal{T}_{TM} :

$$\begin{aligned}
 \mathcal{T}_{TM} = \frac{1}{2e_q} \Bigg\{ & q_z \begin{bmatrix} -\frac{\sqrt{2eBL_i}(\mathcal{M}_{12} + \mathcal{M}_{21})}{E_i + m_e} + \Delta T_{if} \mathcal{M}_{21} & -i\Delta Z_{if} \mathcal{M}_{12} \\ -i\Delta Z_{if} \mathcal{M}_{21} & -\frac{\sqrt{2eBL_i}(\mathcal{M}_{12} + \mathcal{M}_{21})}{E_i + m_e} + \Delta T_{if} \mathcal{M}_{12} \end{bmatrix} \\
 & - 2q_T \mathcal{M}_{22} \begin{bmatrix} \left(\frac{2p_{iz}}{E_i + m_e} - \Delta Z_{if} \right) & -i\Delta T_{if} \\ -i\Delta T_{if} & \left(\frac{2p_{iz}}{E_i + m_e} - \Delta Z_{if} \right) \end{bmatrix} \Bigg\}, \tag{24}
 \end{aligned}$$

$$\mathcal{T}_{TE} = \begin{bmatrix} \frac{\sqrt{2L_i}}{E_i + m_e} (\mathcal{M}_{12} - \mathcal{M}_{21}) + \Delta T_{if} \mathcal{M}_{21} & -\Delta Z_{if} \mathcal{M}_{12} \\ \Delta Z_{if} \mathcal{M}_{21} & -\frac{\sqrt{2L_i}}{E_i + m_e} (\mathcal{M}_{12} - \mathcal{M}_{21}) - \Delta T_{if} \mathcal{M}_{12} \end{bmatrix}. \tag{25}$$

We make numerical calculations with the above formulation.

III. RESULTS

In experiments using electron accelerators it is easier to control Larmor radius R_T of spiral motion electrons than their zOAM L_i . Thus, we present the relationship between R_T and L_i . In the classical mechanics the following relation is satisfied:

$$R_L = \frac{p_T}{eB}, \tag{26}$$

where p_T is the transverse momentum of the initial electron. In the Landau quantization, the transverse momentum p_T is given by $p_T = \sqrt{2eBL_i}$, and we obtain

$$L_i = \frac{eB}{2} R_L^2, \quad R_L = \sqrt{\frac{2L_i}{eB}}. \tag{27}$$

For this expression we write an additional comment. The density distribution in the section (xy plane) of the initial electron

when $n_i = 0$ is written as

$$\begin{aligned}
 \rho_s(r_T) = & \frac{1}{4\pi} e^{-r_T^2/2eB} \\
 & \times \left\{ \frac{1}{(L_i - 1)!} \left(\frac{eBr_T^2}{4} \right)^{L_i - 1} + \frac{1}{L_i!} \left(\frac{eBr_T^2}{4} \right)^{L_i} \right\} \tag{28}
 \end{aligned}$$

with $r_T = \sqrt{x^2 + y^2}$. The root-mean square radius in the section is obtained as

$$\langle r_T^2 \rangle = \frac{1}{2} \int dr_T r_T^2 \rho_s(r_T) = \frac{2L_i + 1}{eB} \approx \frac{2L_i}{eB}. \tag{29}$$

In addition, the peak position of ρ_s is given by $\partial \rho_s / \partial r_T = 0$ and is obtained as

$$(r_T^2)_{\text{peak}} = \frac{2\sqrt{L_i(L_i - 1)}}{eB} \approx \frac{2L_i}{eB}.$$

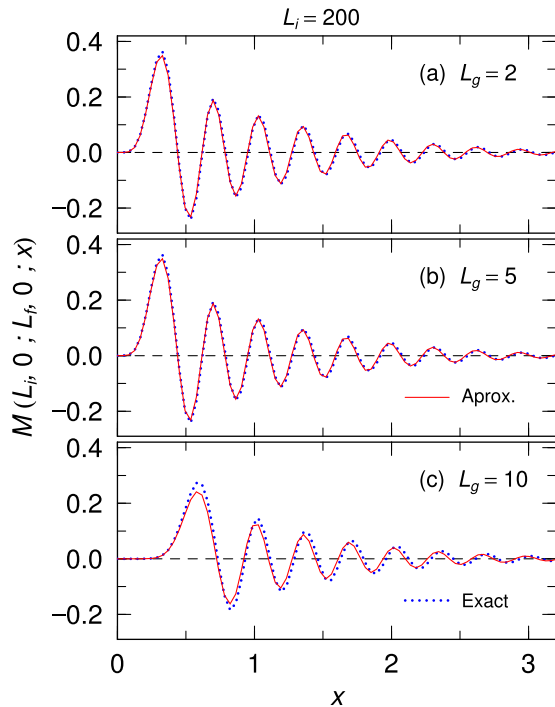


FIG. 1. $\mathcal{M}(L_i, 0; L_f, 0)(x)$ when $L_i = 200$ and $L_i - L_f \equiv L_g = 2$ (a), 5 (b), and 10 (c). The (red) solid and (blue) dotted lines represent the results of the approximate formula (19) and the exact one (15).

The above two estimations lead to the same relation of Eq. (27) when $L_i \gg 1$.

In Fig. 2 we show the photon energy spectrum $d\Gamma_e/d\epsilon_q = (\epsilon_q/q_z)(d\Gamma_e/dq_z)$ of individual modes of photon vortices with m in synchrotron radiations from electrons with a magnetic field strength of $B = 10$ T and a Larmor radius of $R_L = 10 \mu\text{m}$ (L_i of 7.6×10^5). We consider the initial kinetic energy $E_i - m_e = 150$ MeV (a) and 8 GeV (b), and we integrate the decay widths over the xy plane. Note that we discuss the required size and position of the detector later. We see that the energy dependence of the total strengths shows steplike shapes and the dominant mode is clearly separated in each en-

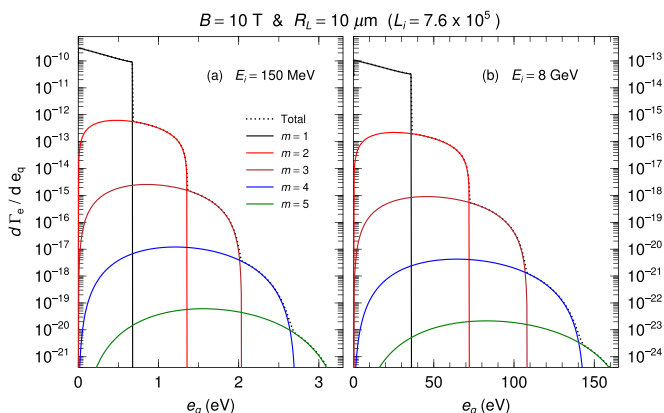


FIG. 2. $d\Gamma_e/d\epsilon_q$ vs the emitted photon energy ϵ_q with the magnetic field strength $B = 10$ T and the Larmor radius $R_L = 10 \mu\text{m}$ when the initial kinetic energy $E_i - m_e = 150$ MeV (a) and 8 GeV (b).

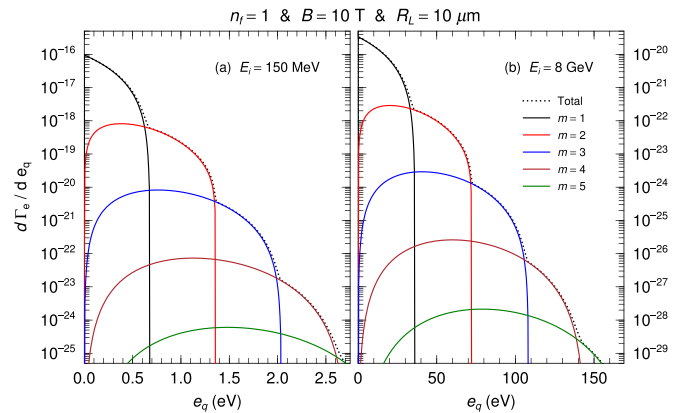


FIG. 3. $d\Gamma_e/d\epsilon_q$ vs the emitted photon energy ϵ_q when $n_f = 1$ at the magnetic field strength $B = 10$ T and the Larmor radius $R_L = 10 \mu\text{m}$ when $E_i - m_e = 150$ MeV (a) and 8 GeV (b),

ergy region. Because the strength decreases by about 10^{-3} as m becomes $m + 1$, the total strengths agree with the strength of the dominant mode for each step. The dominant energy region for the photon vortices with m is between the largest energy for $m - 1$ and that for m as

$$\frac{eB(m-1)}{E_i - p_{iz}} \leq \epsilon_q \leq \frac{eBm}{E_i - p_{iz}}, \quad (30)$$

which is derived from Eq. (13).

As presented previously, it is possible to take a large node number such as $n_f \gg 1$ for the final electron state, corresponding to the shift of the spiral moving axis of an electron after radiation. In Fig. 3 we show the same quantities, but the node number for the final electron state of $n_f = 1$. The contributions from $n_f = 1$ are about 10^{-7} of those from $n_f = 0$; these qualitative behaviors are almost the same as those in the strong magnetic fields [38]. Thus, we can confirm that contributions from $n_f \geq 1$ are negligibly small at least when $m \leq 5$.

Next, we discuss results when the Larmor radius increases. In Fig. 4 we show the photon energy spectrum $d\Gamma_e/d\epsilon_q$ at $B = 10$ T by setting the Larmor radius to be $R_L = 100 \mu\text{m}$

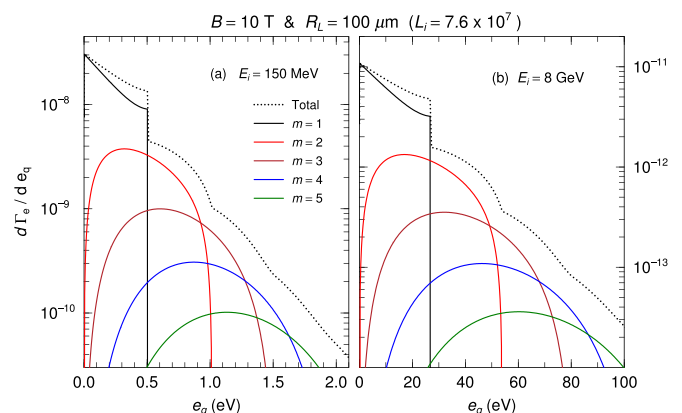


FIG. 4. $d\Gamma_e/d\epsilon_q$ vs the emitted photon energy ϵ_q with the magnetic field strength $B = 10$ T and the Larmor radius $R_L = 100 \mu\text{m}$ when the initial kinetic energy $E_i - m_e = 150$ MeV (a) and 8 GeV (b).

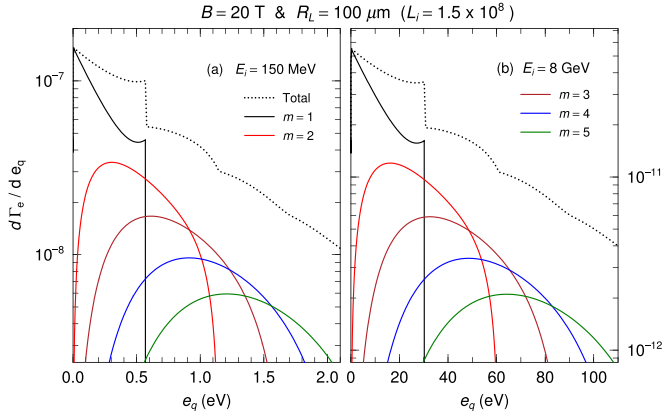


FIG. 5. $d\Gamma_e/d\epsilon_q$ vs the emitted photon energy ϵ_q with the magnetic field strength $B = 20$ T and the Larmor radius $R_L = 100 \mu\text{m}$ when the initial kinetic energy $E_i - m_e = 150$ MeV (a) and 8 GeV (b).

($L_i = 7.6 \times 10^7$) when the initial electron energies are $E_i - m_e = 150$ MeV (a) and 8 GeV (b). We see that the decay widths do not drastically decrease with increase of m ; the peak height at $m + 1$ is about 1/5 of that at m . Then, the decay probabilities of individual modes are not clearly separated in the energy spectrum compared to those for $R_L = 10 \mu\text{m}$. However, we notice that the strengths are much larger than those when $R_L = 10 \mu\text{m}$. In the cases of $m = 2-3$, the strengths for $R_L = 100 \mu\text{m}$ are approximately four to five orders of magnitude larger than those for $R_L = 10 \mu\text{m}$. In addition, the energies of emitted photons are reduced.

In these calculations, we have assumed the magnetic field strength of 10 T. We calculate the energy spectra for 20 T as shown in Fig. 5 by setting the Larmor radius to be $R_L = 100 \mu\text{m}$ ($L_i = 1.5 \times 10^8$) when the initial electron energies are $E_i - m_e = 150$ MeV (a) and 8 GeV (b). These two spectra for 10 and 20 T are similar but the decay widths with $m = 2-3$ for 20 T become larger than those for 10 T by about one order of magnitude. The difference between the decay widths for 10 and 20 T becomes larger as m increases. For $m = 5$, the decay widths for 20 T are approximately 50 larger than those for 10 T. This result suggests that the decay widths are sensitive to the magnetic field strength.

In Fig. 6 we show the kinetic relations between the energy ϵ_q and the transverse momentum q_T for the emitted photons. We see that the transverse momenta satisfy the condition of $q_T \lesssim 6$ meV. When $B = 10$ T, we obtain $\sqrt{eB} = 24.3$ eV and $q_T^2/eB \approx 10^{-8}$. Then, the value of the argument of the Bessel function in Eq. (18) is $\sqrt{2L_i q_T^2/eB} \approx 10^{-1}$. This fact shows us that this approximation is confirmed to be available in the present calculations although this approximation is not applicable when the argument is very large. Furthermore, we can know several features of the generated photons in the present paper. First, in this figure, the energy region for the emitted photons with a fixed m becomes broader when the initial electron energy increases, and it becomes narrower when the Larmor radius of the initial electron increases. We here define $E_{iT} \equiv \sqrt{2eBL_i + m_e^2}$ and obtain the relationships of $p_{iz} \approx E_i$ and $E_i - p_{iz} \approx E_{iT}^2/2E_i$. Using these, Eq. (13) approximately

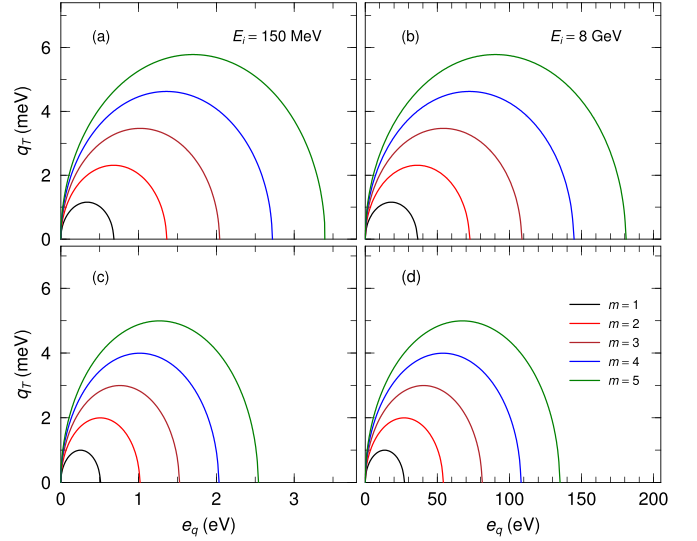


FIG. 6. The transverse momentum q_T vs the energy ϵ_q of the emitted photon when $B = 10$ T. The results when $E_i - m_e = 150$ MeV and $R_L = 10 \mu\text{m}$ are shown in the upper left panel (a), those when $E_i - m_e = 8$ GeV and $R_L = 10 \mu\text{m}$ are shown in the upper right panel (b), those when $E_i - m_e = 150$ MeV and $R_L = 100 \mu\text{m}$ are shown in the lower left panel (c), and those when $E_i = 8$ GeV and $R_L = 100 \mu\text{m}$ are shown in the lower right panel (d).

becomes

$$\frac{m_e B}{2E_i} \lesssim \epsilon_q \lesssim \frac{2m_e B E_i}{E_{iT}^2} = \frac{2mE_i}{2L_i + m_e^2/eB}. \quad (31)$$

The lower boundary of this energy region is almost zero because of $m\sqrt{eB} \ll E_i$, and the upper boundary is proportional to the initial energy E_i . In the present calculations the ratio of the assumed electron energies is $8 \text{ GeV}/150 \text{ MeV} = 53.3$ and the upper boundary indeed corresponding to each m follows this ratio. In addition, we can know that the upper boundary decreases as the L_i increases. When $B = 10$ T and $m_e^2/eB \approx 4.41 \times 10^8$, the ratio of the upper boundaries for the two different L_i is $E_{iT}^2(L_i = 7.6 \times 10^5)/E_{iT}^2(L_i = 7.6 \times 10^7) \approx 0.75$, which agrees with the ratio of the energy region size between the two Larmor radii of $R_L = 10$ and 100 corresponding to $L_i = 7.6 \times 10^5$ and 7.6×10^7 , respectively. Second, we see that as the z TAM m increases the energy ϵ_q and the transverse momentum q_T of the emitted photon increase and that the maximum value of q_T is approximately proportional to m though the ratio of the energy to the transverse momentum is kept on the order of about $q_T/\epsilon_q \approx 10^{-3}$. When $E_i \gg E_{iT}$ and $\epsilon_q \gg q_T$,

$$\begin{aligned} q_T^2 &= (E_i - E_f)^2 - (p_{iz} - p_{fz})^2 \\ &= -E_{iT}^2 + E_{fT}^2 + 2e_q(E_i - p_{iz}) + 2p_{iz}(e_q - q_z) \\ &\approx -E_{iT}^2 + E_{fT}^2 + \frac{E_i q_T^2}{e_q}, \end{aligned} \quad (32)$$

and then we obtain

$$q_T^2 \approx \frac{e_q}{E_i - e_q} (E_{iT}^2 - E_{fT}^2) \approx \frac{2eB e_q}{E_i} (L_i - L_f). \quad (33)$$

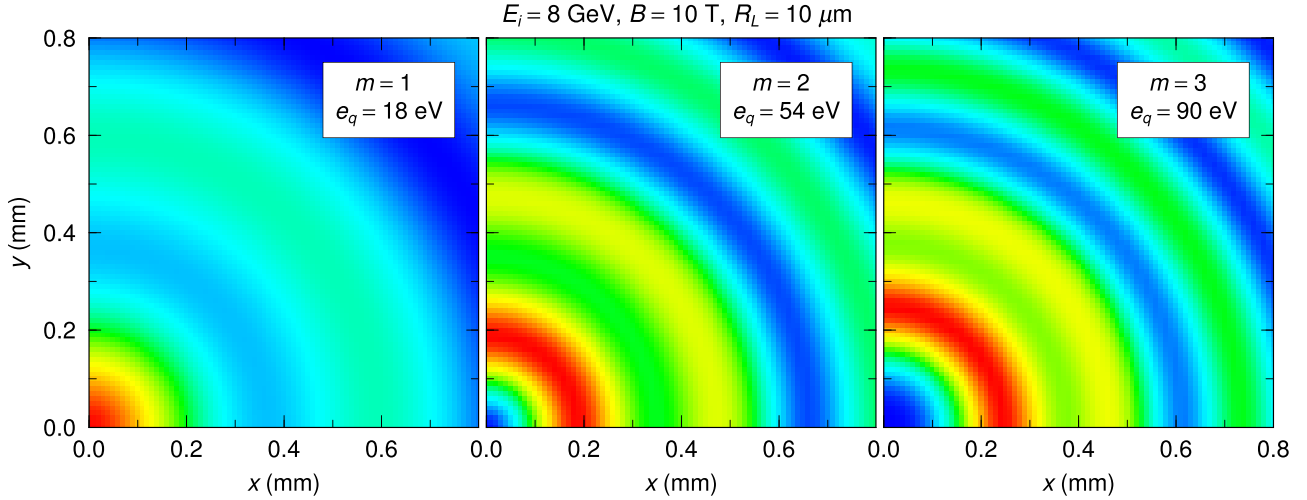


FIG. 7. Contour plots for the areal density distribution of the emitted photon with $m = 1$ and $e_q = 18.1$ eV (a), $m = 2$ and $e_q = 54.2$ eV (b), and $m = 3$ and $e_q = 90.3$ eV (c) when $B = 10$ T, $E_i - m_e = 8$ GeV, and $R_L = 10$ μm . The density increases in the order of blue, cyan, green, yellow, and red.

Although an emitted photon includes three components of zOAM, $L_i - L_f$ and $L_i - L_f \pm 1$, we can approximately consider $m \approx L_i - L_f$. Because of Eq. (31) we obtain $e_q/E_i \propto eBm/E_{iT}^2$ and

$$q_T \approx \sqrt{\frac{2eBe_q m}{E_i}} \propto \frac{eB}{E_{iT}} m. \quad (34)$$

Thus, the above analysis explains the qualitative behaviors of the kinematical relations for the emitted photon momenta when $E_i \gg E_{iT}$.

We here consider the areal density of generated photon vortices in the plane perpendicular to the beam axis (xy plane). The areal density of radiated photon number per time period Δt can be calculated in the equation

$$N_\gamma^{(a)} = \frac{J_e \Delta t}{e} \left(\frac{1}{\hbar} \frac{\partial \Gamma_e^{(a)}}{\partial e_q} \Delta e_q \right) \Delta t = \frac{J_e}{e} \left(\frac{1}{\hbar c} \frac{\partial \Gamma_e^{(a)}}{\partial e_q} \Delta e_q \right) c \Delta t^2, \quad (35)$$

where J_e is a current of the incident electron, and Δe_q is the energy width of the measured photon. The wave functions of photon vortices (Bessel waves) distribute in large regions in the xy plane. The strength distributions of the Bessel waves in the xy plane are given by

$$\begin{aligned} |A_m^{(\text{TE})}(\mathbf{r}_T)|^2 &= \frac{1}{2} |J_{m+1}(q_T r_T)|^2 + \frac{1}{2} |J_{m-1}(q_T r_T)|^2, \quad (36) \\ |A_m^{(\text{TM})}(\mathbf{r}_T)|^2 &= \frac{q_z^2}{2e_q^2} [|J_{m+1}(q_T r_T)|^2 + |J_{m-1}(q_T r_T)|^2] \\ &\quad + \frac{q_T^2}{e_q^2} |J_m(q_T r_T)|^2, \quad (37) \end{aligned}$$

and the areal density of the produced photons per time period Δt is estimated as

$$\rho_\gamma(r_T) = \frac{1}{\pi R_T^2} \{ N_\gamma^{(\text{TE})} |A^{(\text{TE})}(r_T)|^2 + N_\gamma^{(\text{TM})} |A^{(\text{TM})}(r_T)|^2 \}. \quad (38)$$

As an example, we take the electron current to be $J_e = 1$ mA, the magnetic field strength to be $B = 10$ T, the measuring time to be $\Delta t = 1$ s, the energy width to be $\Delta e_q = 0.1$ eV, and the Larmor radius to be $R_T = 10$ μm . In Fig. 7 we show the contour plots of the averaged photon density in the plane perpendicular to the beam direction. We take the photon energy to be $e_q = (m - 1/2)/(E_i - p_{iz})$, that is near the center value in the energy region Eq. (30). The distribution of $|A|^2$ has a peak at the center ($x = y = 0$) when $m = 1$. On the other hand, when $m = 2, 3$ their photon densities vanish around the center. This is one of the features of the photon vortex. In Fig. 8 we show the number density of emitted photons ρ_γ as a function of r_T . These distributions are written as a superposition of the three Bessel functions $J_m(r_T)$ ($m = N - 1, N, N + 1$) and exhibit complicated behavior of r_T dependence. In this figure we can see that the density becomes zero at $r_T = 0$ when $m \geq 2$, and that the r_T dependences of $E_i - m_e = 150$ MeV and 8 GeV show the same behaviors except for the absolute values. This is consistent with the results for the energy spectra; the qualitative behaviors are almost independent of the initial electron energy although the absolute values are different. The densities of the initial and final electrons are distributed to infinite r_T and the oscillation behaviors of the photon strengths also continue to infinity. In experiments in the laboratory, however, the electron densities are distributed in an area limited by the size of a magnetic field, and the densities of produced photons also appear in a limited range. The formulation in this paper is valid, but it would not be very meaningful to see the behavior of vibrations at a far distance. Figure 8 shows that the oscillation behavior can be observed in order of several hundred μm . The wave functions of emitted photons travel parallel to the magnetic field after radiation, and thus the areal density does not depend on the distance from the magnetic field. Furthermore, Fig. 8 shows that the amplitude decreases with increasing r_T without the oscillation. This result shows that when a detector with a size of a few cm is set on the axis of the spiral motion electrons, the energy spectra nearly equal to those presented in Figs. 2, 4, and 5 can be measured. The present paper clearly shows

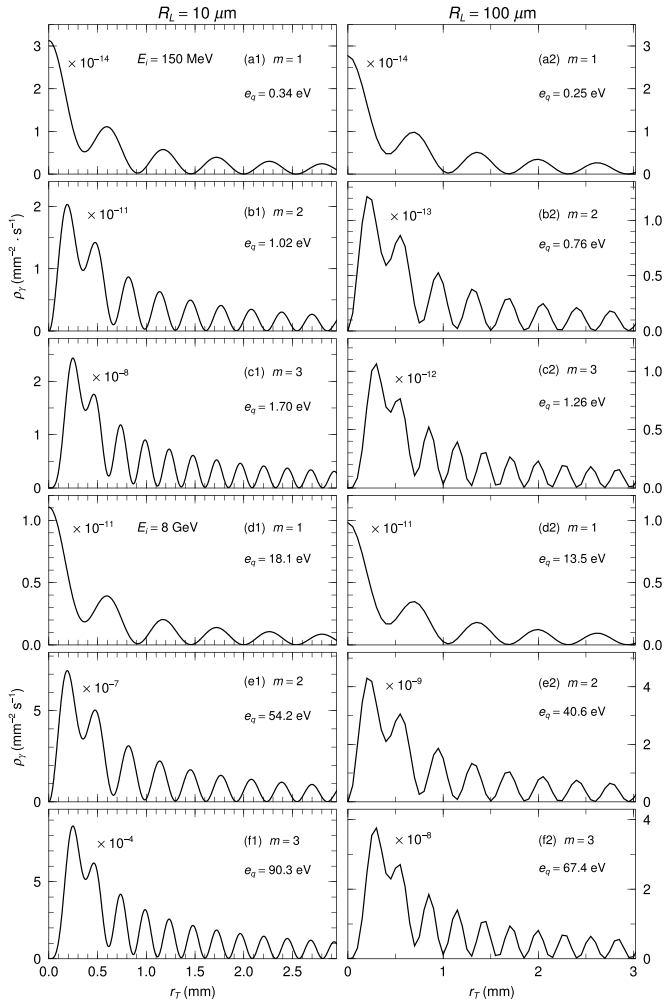


FIG. 8. Density distribution of emitted photon per second as a function of the distance from the rotation axis with $m = 1$ (a), $m = 2$ (b), and $m = 3$ (c) when $E_i - m_e = 150$ GeV, and those with $m = 1$ (d), $m = 2$ (e), and $m = 3$ (f) when $E_i - m_e = 8$ GeV. In all the calculations $B = 10$ T and $R_L = 10$ and $100 \mu\text{m}$.

that when one controls the entrance trajectory and energy of an electron beam under a uniform magnetic field one can generate predominantly photon vortices with a specific zTAM in a limited energy range. This is useful for various applications at the quantum level such as quantum control and quantum communication.

Finally, we discuss a possibility of generation of coherent photon vortices. Our previous study [38] and the present paper show that photon vortices are generated by harmonic radiations under uniform magnetic fields but there is no coherent structure at the macrolevel. This suggests that even if one cannot observe the optical vortex at the macrolevel it is possible to observe the effect of the large angular momentum transfer in interactions of each photon vortex with an object. In contrast, when an optical vortex consisting of photons that are not

the eigenstates of zTAM interacts on materials it is difficult to observe such quantum effects. The third possibility is an optical vortex consisting of photon vortices, namely coherent photon vortices. In the present method, when one uses an electron bunch with size much shorter than a wavelength of the oscillation in the areal density in Fig. 8 and the wavelength of the harmonic radiation, it is expected to generate coherent photon vortices. Note, however, that in such condition the synchrotron radiation may be largely different from the present calculation because of the effect of the entrance of electrons to the magnetic field.

IV. SUMMARY

In quantum theory, electron orbitals in a magnetic field are under Landau states and synchrotron radiation is treated as a transition between two Landau levels. The level density increases as the magnetic field strength decreases, and it becomes too high to calculate exactly synchrotron radiation in possible magnetic field strengths on the ground. In this paper we have developed a formulation for generation of photon vortices by synchrotron radiation from a spiral motion electron in a uniform magnetic field with feasible parameters in the laboratory by using asymptotic formulations of the emission amplitudes under the condition of $L_i - L_f \ll L_i$. This approximation is applicable for photon vortex production of zTAM of up to several tens of \hbar . Then, to present the expected energy spectra and areal densities of generated photon vortices we calculate numerically those of photon vortices for 150-MeV and 8-GeV electron energies and a magnetic field of 10 and 20 T. We set Larmor radii of $R_L = 10$ and $100 \mu\text{m}$ for electron spiral motion. The energy spectra show that the photons have a clearly defined energy region for each zTAM. The calculated areal densities present oscillation structures as a function of r_T , depending on the photon energy and zTAM. When one places a detector with a diameter of a few cm on the axis of the spiral motion, one can observe an energy spectrum approximately equal to that obtained by the calculation for the assumed conditions. These results indicate that it is possible to generate predominantly photon vortices using synchrotron radiations and to control their zTAM when one controls the energy and entrance trajectory of the electrons and the structure of the magnetic field. The present formula contributes to the prediction and verification of photon vortex generation.

ACKNOWLEDGMENTS

This work was supported by Grants-in-Aid for Scientific Research of Japan Society for the Promotion of Science (Grants No. JP19K03833, No. JP20K03958, No. JP22H03881, and No. JP22H01239). M.K.C. was supported by the National Research Foundation of Korea (Grants No. NRF-2020R1A2C3006177 and No. NRF-2021R1A6A1A03043957). T.K. was supported in part by the National Key Research and Development Program of China (Grant No. 2022YFA1602401).

[1] L. Allen, M. W. Beijersbergen, R. J. C. Spreeuw, and J. P. Woerdman, Orbital angular momentum of light and the trans-

formation of Laguerre-Gaussian laser modes, *Phys. Rev. A* **45**, 8185 (1992).

- [2] U. D. Jentschura and V. G. Serbo, Generation of high-energy photons with large orbital angular momentum by Compton, *Phys. Rev. Lett.* **106**, 013001 (2011).
- [3] V. Petrillo, G. Dattoli, I. Drebot, and F. Nguyen, Compton scattered x-gamma rays with orbital momentum, *Phys. Rev. Lett.* **117**, 123903 (2016).
- [4] J. A. Sherwin, Theoretical study of the double Compton effect with twisted photons, *Phys. Rev. A* **95**, 052101 (2017).
- [5] A. A. Peshkov, A. V. Volotka, A. Surzhykov, and S. Fritzsche, Rayleigh scattering of twisted light by hydrogenlike ions, *Phys. Rev. A* **97**, 023802 (2018).
- [6] T. Maruyama, T. Hayakawa, and T. Kajino, Compton scattering of γ -ray vortex with laguerre Gaussian wave function, *Sci. Rep.* **9**, 51 (2019).
- [7] J. Wang, J.-Y. Yang, I. M. Fazal, N. Ahmed, Y. Yan, H. Huang, Y. Ren, Y. Yue, S. Dolinar, M. Tur, and A. E. Willner, Terabit free-space data transmission employing orbital angular momentum multiplexing, *Nat. Photonics* **6**, 488 (2012).
- [8] K. Toyoda, F. Takahashi, S. Takizawa, Y. Tokizane, K. Miyamoto, R. Morita, and T. Omatsu, Transfer of light helicity to nanostructures, *Phys. Rev. Lett.* **110**, 143603 (2013).
- [9] N. Bozinovic, Y. Yue, Y. Ren, M. Tur, P. Kristensen, H. Huang, A. E. Willner, and S. Ramachandran, Terabit-scale orbital angular momentum mode division multiplexing in fibers, *Science* **340**, 1545 (2013).
- [10] H. He, M. E. J. Friese, N. R. Heckenberg, and H. Rubinsztein-Dunlop, Direct observation of transfer of angular momentum to absorptive particles from a laser beam with a phase singularity, *Phys. Rev. Lett.* **75**, 826 (1995).
- [11] A. A. Sirenko, P. Marsik, C. Bernhard, T. N. Stanislavchuk, V. Kiryukhin, and S.-W. Cheong, Terahertz vortex beam as a spectroscopic probe of magnetic excitations, *Phys. Rev. Lett.* **122**, 237401 (2019).
- [12] T. Omatsu, K. Miyamoto, K. Toyoda, R. Morita, Y. Arita, and K. Dholakia, A new twist for materials science: The formation of chiral structures using the angular momentum of light, *Adv. Opt. Mater.* **7**, 180672 (2019).
- [13] A. E. Willner, K. Pang, H. Song, K. Zou, and H. Zhou, Orbital angular momentum of light for communications, *Appl. Phys. Rev.* **8**, 041312 (2021).
- [14] F. Tamburini, B. Thidé, G. Molina-Terriza, and G. Anzolin, Twisting of light around rotating black holes, *Nat. Phys.* **7**, 195 (2011).
- [15] S. Sasaki and I. McNulty, Proposal for generating brilliant x-ray beams carrying orbital angular momentum, *Phys. Rev. Lett.* **100**, 124801 (2008).
- [16] J. Bahrtdt, K. Holldack, P. Kuske, R. Müller, M. Scheer, and P. Schmid, First observation of photons carrying orbital angular momentum in undulator radiation, *Phys. Rev. Lett.* **111**, 034801 (2013).
- [17] E. Hemsing, M. Dunning, C. Hast, T. Raubenheimer, and Dao Xiang, First characterization of coherent optical vortices from harmonic undulator radiation, *Phys. Rev. Lett.* **113**, 134803 (2014).
- [18] M. Katoh, M. Fujimoto, N. S. Mirian, T. Konomi, Y. Taira, T. Kaneyasu, M. Hosaka, N. Yamamoto, A. Mochihashi, Y. Takashima, K. Kuroda, A. Miyamoto, K. Miyamoto, and S. Sasaki, Helical phase structure of radiation from an electron in circular motion, *Sci. Rep.* **7**, 6130 (2017).
- [19] M. Katoh, M. Fujimoto, H. Kawaguchi, K. Tsuchiya, K. Ohmi, T. Kaneyasu, Y. Taira, M. Hosaka, A. Mochihashi, and Y. Takashima, Angular momentum of twisted radiation from an electron in spiral motion, *Phys. Rev. Lett.* **118**, 094801 (2017).
- [20] O. V. Bogdanov, P. O. Kazinski, and G. Yu. Lazarenko, Probability of radiation of twisted photons by classical currents, *Phys. Rev. A* **97**, 033837 (2018).
- [21] O. V. Bogdanov, P. O. Kazinski, and G. Yu. Lazarenko, Semi-classical probability of radiation of twisted photons in the ultrarelativistic limit, *Phys. Rev. D* **99**, 116016 (2019).
- [22] D. V. Karlovets, S. S. Baturin, G. Geloni, G. K. Sizykh, and V. G. Serbo, Generation of vortex particles via generalized measurements, *Eur. Phys. J. C* **82**, 1008 (2022).
- [23] E. Hemsing, A. Knyazik, M. Dunning, D. Xiang, A. Marinelli, C. Hast, and J. B. Rosenzweig, Coherent optical vortices from relativistic electron beams, *Nat. Phys.* **9**, 549 (2013).
- [24] P. Rebernik Ribič, B. Rosner, D. Gauthier, E. Allaria, F. Doring, L. Foglia, L. Giannessi, N. Mahne, M. Manfredda, C. Masciovecchio, R. Mincigrucci, N. Mirian, E. Principi, E. Roussel, A. Simoncig, S. Spampinati, C. David, and G. DeNinno, Extreme-ultraviolet vortices from a free-electron laser, *Phys. Rev. X* **7**, 031036 (2017).
- [25] A. Mair, A. Vaziri, G. Weihs, and A. Zeilinger, Entanglement of the orbital angular momentum states of photons, *Nature (London)* **412**, 313 (2001).
- [26] J. Leach, M. J. Padgett, S. M. Barnett, S. Franke-Arnold, and J. Courtial, Measuring the orbital angular momentum of a single photon *Phys. Rev. Lett.* **88**, 257901 (2002).
- [27] M. Babiker, C. R. Bennett, D. L. Andrews, and L. C. D. Romero, Orbital angular momentum exchange in the interaction of twisted light with molecules, *Phys. Rev. Lett.* **89**, 143601 (2002).
- [28] A. Alexandrescu, D. Cojoc, and E. I. DiFabrizio, Mechanism of angular momentum exchange between molecules and Laguerre-Gaussian beams, *Phys. Rev. Lett.* **96**, 243001 (2006).
- [29] A. Picón, A. Benseny, J. Mompart, J. R. Vázquez de Aldana, L. Plaja, G. F. Calvo, and L. Roso, Transferring orbital and spin angular momenta of light to atoms, *New J. Phys.* **12**, 083053 (2010).
- [30] A. Afanasev, C. E. Carlson, and A. Mukherjee, Off-axis excitation of hydrogenlike atoms by twisted photons, *Phys. Rev. A* **88**, 033841 (2013).
- [31] A. Afanasev, V. G. Serbo, and M. Solyanik, Radiative capture of cold neutrons by protons and deuteron photodisintegration with twisted beams, *J. Phys. G* **45**, 055102 (2018).
- [32] Y. Taira, T. Hayakawa, and M. Katoh, Gamma-ray vortices from nonlinear inverse Thomson scattering of circularly polarized light, *Sci. Rep.* **7**, 5018 (2017).
- [33] R. Jáuregui and S. Hacyan, Quantum-mechanical properties of Bessel beams, *Phys. Rev. A* **71**, 033411 (2005).
- [34] Y. Y. Chen, J. X. Li, K. Z. Hatsagortsyan, and C. H. Keitel, Gamma-ray beams with large orbital angular momentum via nonlinear Compton scattering with radiation reaction, *Phys. Rev. Lett.* **121**, 074801 (2018).
- [35] X. X. Zhu, M. Chen, T. P. Yu, S. M. Weng, K. X. Hu, P. McKenna, and Z. M. Sheng, Bright attosecond c-ray pulses from nonlinear Compton scattering with laser-illuminated compound targets, *Appl. Phys. Lett.* **112**, 174102 (2018).

- [36] S. Mereghetti, The strongest cosmic magnets: Soft gamma-ray repeaters and anomalous x-ray pulsars, *Astron. Astrophys. Rev.* **15**, 225 (2008).
- [37] J. C. McKinney, A. Tchekhovskoy, and R. D. Blandford, Alignment of magnetized accretion disks and relativistic jets with spinning black holes, *Science* **339**, 49 (2013).
- [38] T. Maruyama, T. Hayakawa, T. Kajino, and M.-K. Cheoun, Generation of photon vortex by synchrotron radiation from electrons in Landau states under astrophysical magnetic fields, *Phys. Lett. B* **826**, 136779 (2022).
- [39] V. G. Bezchastnov and G. G. Pavlov, Quantum relativistic theory of the synchrotron/cyclotron radiation in a strongly-magnetized plasma: The case of longitudinal propagation, *Astrophys. Space Sci.* **148**, 257 (1988).
- [40] G. G. Pavlov, V. G. Bezchastnov, P. Mészáros, and S. G. Alexander, Radiative widths and splitting of cyclotron lines in superstrong magnetic fields, *Astrophys. J.* **380**, 541 (1991).
- [41] V. G. Bagrov, Quantum theory of synchrotron radiation, in *Synchrotron Radiation Theory and its Development*, edited by V. A. Bordovitsyn (World Scientific, Singapore, 1999), pp. 121–178.
- [42] O. F. Dorofeyev, A. V. Borisov, and V. Ch. Zhukovsky, Synchrotron radiation in a strong magnetic field, in *Synchrotron Radiation Theory and its Development*, edited by V. A. Bordovitsyn (World Scientific, Singapore, 1999), pp. 347–383.
- [43] G. S. Bisnovatyi-Kogan, Synchrotron radiation in astrophysics, in *Synchrotron Radiation Theory and its Development*, edited by V. A. Bordovitsyn (World Scientific, Singapore, 1999), pp. 385–443.
- [44] T. N. Wistisen, Quantum synchrotron radiation in the case of a field with finite extension, *Phys. Rev. D* **92**, 045045 (2015).
- [45] K. van Kruining, F. Mackenroth, and J. B. Götte, Radiative spin polarization of electrons in an ultrastrong magnetic field, *Phys. Rev. D* **100**, 056014 (2019).
- [46] R. Kubo, S. J. Miyake, and N. Hashitsume, Quantum theory of galvanomagnetic effect at extremely strong magnetic fields, *Solid State Phys.* **17**, 269 (1965).
- [47] R. Álvarez-Nodarse and J. J. Moreno-Balcázar, Asymptotic properties of generalized Laguerre orthogonal polynomials, *Indagationes Math.* **15**, 151 (2004).